Provided for non-commercial research and education use.
Not for reproduction, distribution or commercial use.

This article appeared in a journal published by Elsevier. The attached copy is furnished to the author for internal non-commercial research and education use, including for instruction at the authors institution and sharing with colleagues.

Other uses, including reproduction and distribution, or selling or licensing copies, or posting to personal, institutional or third party websites are prohibited.

In most cases authors are permitted to post their version of the article (e.g. in Word or Tex form) to their personal website or institutional repository. Authors requiring further information regarding Elsevier's archiving and manuscript policies are encouraged to visit:

http://www.elsevier.com/authorsrights

Author's personal copy

International Journal of Heat and Mass Transfer 65 (2013) 713–718

Contents lists available at SciVerse ScienceDirect

International Journal of Heat and Mass Transfer

journal homepage: www.elsevier.com/locate/ijhmt

A study of near-infrared nanosecond laser ablation of silicon carbide

Doan Hong Duc *, Iwatani Naoki, Fushinobu Kazuyoshi

Tokyo Institute of Technology, Box I6-3, Meguro-ku, Tokyo 152-8550, Japan

ARTICLE INFO

Article history:
Received 31 July 2012
Accepted 20 June 2013

Keywords:
Laser ablation
Silicon carbide
Ablation threshold
Free carrier absorption

ABSTRACT

This work presents a fundamental study about ablation threshold, absorption coefficient and absorption mechanism of silicon carbide (SiC) in the laser drilling process. Experimental study has been performed on single infrared (1064 nm) ns pulse laser ablation of SiC at various fluence values. Hole diameters were measured to predict the absorption threshold. Based on the ablation threshold, an average absorption coefficient of SiC at infrared wavelength during the laser ablation process is calculated. The result is discussed based on absorption coefficient dependence on doping concentration and temperature in semiconductor. A preliminary model is proposed that accounts for the heat conduction and surface evaporation to predict the cross-sectional shape of drilling hole. Analytical modeling results are in good agreement with observed features produced from the laser. The paper will conclude with suggestions for further research and potential applications for the work.

© 2013 Elsevier Ltd. All rights reserved.

1. Introduction

The success of microelectronics has been followed by rapid development in microelectro-mechanical systems (MEMS) where silicon (Si) is currently the leading material. Nowadays there is an increased demand for devices capable of functioning at high temperatures and in harsh environments, which exceed the physical properties of Si. This demand accounts for the emergence of SiC, with higher band-gap, higher breakdown threshold, higher thermal conductivity and higher saturation velocity than Si, as preferred material for MEMS in the future.

Unfortunately some of these properties of SiC are also barriers to the fabrication of microelectronics and MEMS devices. Conventional dry etching techniques of via through SiC wafers requires time-consuming mechanical thinning to a thickness of ~100 μm. Typical etch rates for 4H and 6H SiC substrates in F_2- or Cl_2-based plasmas range between 0.2 μm/min and 1.3 μm/min [1–4]. In contrast to the chemical-based micro-fabrication methods, laser ablation of SiC is capable of higher etching rates [5–7] and precise control of via size with advancement of the reduction in the number of processing steps as masking, machining independent of crystal structure, and curved surfaces. Laser ablation of SiC has been carried out with pulse durations from nanosecond to femtosecond regime. Femtosecond lasers have produced little contamination and low HAZ [8–10]. However, the lower etch rates via formation compared with nanosecond laser and the high cost of machining system still are the problem to spread out. In the practical system, the ns pulse laser machining is widely used.

Single-crystalline SiC is practically transparent at visible wavelengths, but has an optical absorption on the order of $10^5\ cm^{-1}$ in the UV regime due to the intrinsic absorption of photon energy. Nanosecond pulsed UV lasers such as excimer and frequency tripled and quadrupled Nd:YAG are the most widely used [11–14] due to their prevalence and the high optical absorption of crystalline SiC at UV wavelengths. It is concluded that UV laser ablation is an effective but slow material removal process for SiC wafers compared to infrared lasers such as 1064 nm Nd:YAG [14]. Although the advantages of low cost and high speed material removal process, the important parameters such as ablation threshold, absorption coefficient for near-infrared laser ablation of SiC are still very limited. This work presents a fundamental study about near-infrared laser ablation threshold, absorption coefficient and absorption mechanism of SiC in the laser drilling process experimentally and theoretically.

2. Estimating ablation threshold and absorption coefficient

In this section, an experiment to estimate the ablation threshold and absorption coefficient of SiC is carried out. First, the method by using the diameters of drilled vias and applied energy of laser pulses [15] is discussed. Assuming that the laser pulse has a Gaussian spatial distribution:

$$F(r) = F_0 \exp\left(\frac{-2r^2}{r_0^2}\right) \tag{1}$$

$$F_0 = \frac{2E}{\pi r_0^2} \tag{2}$$

* Corresponding author. Tel./fax: +81 3 5734 2500.
E-mail address: doan.d.aa@m.titech.ac.jp (D.H. Duc).

0017-9310/$ - see front matter © 2013 Elsevier Ltd. All rights reserved.
http://dx.doi.org/10.1016/j.ijheatmasstransfer.2013.06.050

Author's personal copy

Nomenclature

c	speed of light, m/s
e	electron charge, C
E	pulse energy, J
f	focal length, m
F	laser fluence, J/cm^2
F_0	peak fluence at the beam center, J/cm^2
F_{th}	ablation threshold, J/cm^2
h	enthalpy per unit volume, J/m^3
H_{latent}	latent energy density, J/m^3
$H_{removal}$	removal energy density, J/m^3
H_{sens}	sensible energy density, J/m^3
I_0	laser intensity, W/m^2
k	thermal conductivity, W/(m K)
k_B	Boltzmann constant, J/K
L	thickness of SiC wafer, m
L_m	latent heat of melting, J/atom
L_v	latent heat of vaporization, J/atom
m^*	charge carrier effective mass, kg
N_D	impurity concentration, m^{-3}
n	refractive index of SiC
P	laser power, W
P_a	ambient pressure, Pa
r	radial distance
r_0	beam radius, m
R	reflectivity
R_v	universal gas constant, J/(mol K)
s	volumetric heat generation rate, W/m^3
t_0	pulse width, ns
T	temperature, K
T_∞	ambient temperature, K
T_m	melting temperature, K
T_c	critical temperature, K
T_s	surface temperature, K
v_s	surface velocity, m/s
z	axial distance, m
z_s	surface distance, m

Greek symbols

α	absorption coefficient, cm^{-1}
ε_0	permittivity, F/m
λ	laser beam wavelength, nm
μ	electron mobility, cm^2/(V s)
ρ	density of liquid medium, kg/m^3
ρ_l	density of liquid silicon, kg/m^3
ρ_s	density of solid SiC, kg/m^3
ω	beam waist of the laser before lens, m

Here r, F_0 and E are beam radius, peak fluence at the beam center and the pulse energy, respectively. If the laser pulse ablates the SiC only when the fluence is above the ablation threshold, the relationship between the diameters of ablation hole and the ablation threshold is following:

$$D^2 = 2r_0^2 \ln\left(\frac{F_0}{F_{th}}\right) \tag{3}$$

Here D and F_{th} are the diameter of the single shot ablated via and ablation threshold value, respectively. Substituting for the peak fluence from Eq. (2)

$$D^2 = 2r_0^2 \ln(E) - 2r_0^2 \ln\left(\frac{\pi r_0^2 F_{th}}{2}\right) \tag{4}$$

By fitting the relationship between the diameters of ablation hole and applied energy of laser pulses, the spot size of the laser pulse can be obtain from the slope of the graph of D^2 versus ln(E). Using the spot size and the intercept of the same graph, the threshold fluence can be found.

A commercial 4H–SiC wafer ($10 \times 10 \times 0.34$ mm) was used for laser drilling. The SiC sample is doped with nitrogen. The concentration of nitrogen was measured by using secondary ion mass spectrometry method as the depth-wise profile of concentration and shown in Fig. 1 with concentration of 1.8×10^{20} cm^{-3} at the surface and 1.6×10^{19} cm^{-3} in the bulk.

The infrared nanosecond laser used in this work was an Nd:YAG laser (Continuum Surelite I-10, $P = 4.72$ W, $\lambda = 1064$ nm) with the pulse duration of 6 ns. The laser is operated in the TEM$_{00}$ mode, and the laser beam profile is Gaussian, which was measured by a CCD camera. The pulse energy was controlled by an external attenuator including a variable beam splitter and a correction plate. After focused by a 10× object lens, pulse energies were measured by using a energy meter.

At each of different pulse energy level, single shot ablation experiment was carried out 5 times. The relationship between the diameters of drilled holes and applied energy of laser pulses was shown in Fig. 2. The plot points show the average experimental values. The under and upper error bars show the minimum and the maximum values of via diameter among the 5 experimental values. As shown in Fig. 2, a straight line can be fitted to represent a low energy regime and the other straight line represents a high energy regime. At low energy regime, the surface evaporation is weak, effect of plasma shielding can be ignored, and the use of Eq. (4) is acceptable. However, at high energy regime surface evaporation become stronger, effect of plasma shielding is more significant and the Eq. (4) can no longer be used. Therefore, in this experiment the results in the low energy regime are used. Estimated spot size and ablation threshold are: $r_0 = 13.6$ µm and $F_{th} = 7.8$ J/cm^2, respectively. The estimated spot size value shows a good agreement with the diffraction-limited spot size, which was calculated as

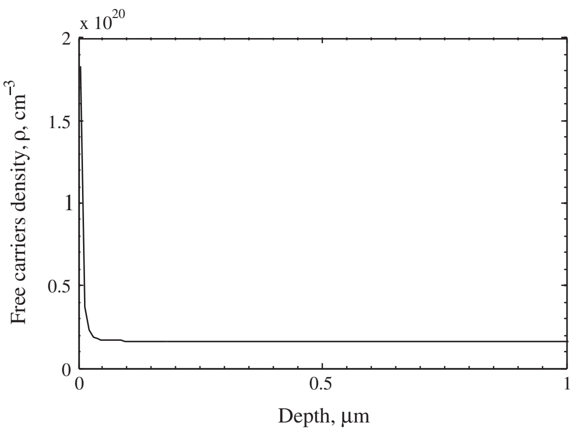

Fig. 1. Depth profile of nitrogen concentration measured by using secondary ion mass spectrometry.

Author's personal copy

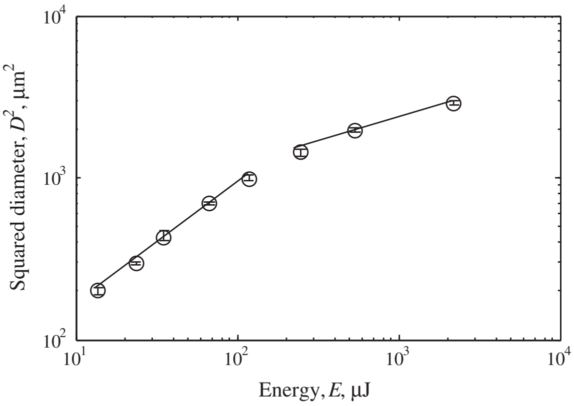

Fig. 2. Plot of squared diameter against energy per pulse.

$$r_0 = \frac{M^2 \lambda f}{\pi \omega} = 14.6\ \mu\text{m} \tag{5}$$

Here λ, f and ω are the wavelength, focal length and the beam waist of the laser before lens, respectively. The ablation threshold value is lagerer the values of 1.17 J/cm^2 found in Ref. [16] should be caused by different absorption coefficient, which strongly depends on nitrogen doping concentration of SiC wafer.

In order to estimate the absorption coefficient of the solid SiC, the relationship among the ablation threshold, sensible energy, latent energy and the removal energy is considered. It is assumed that the interaction time between laser pulse and material is short enough to neglect the heat loss by the heat conduction. The ablation threshold value can be expressed as a sum of energy density required for heating up solid SiC from room temperature to the melting temperature, latent and removal energy, as showns in Eq. (6):

$$F_{\text{th}} = \alpha_s^{-1}(H_{\text{sens}} + H_{latent}) + \alpha_l^{-1} H_{\text{removal}} \tag{6}$$

Here α_s and α_l are the absorption coefficient of solid and liquid SiC, respectively. Removal energy and the sum of the sensible and latent energy have a same order [25]. While on the other hand, absorption coefficient of liquid SiC is 2 orders higher than that of solid [17]. Therefore, the second term in Eq. (6) is small compared with the first term and can be neglected as

$$F_{\text{th}} \approx \alpha_s^{-1}(H_{\text{sens}} + H_{latent}) \tag{7}$$

As shown in Eq. (7), the ablation threshold value of SiC is governed by absorption coefficient of solid SiC, which should strongly depends on the dopant concentration and temperature in the infrared wavelength regime. By using Eq. (7), the absorption coefficient of solid SiC can be obtained as $\alpha_s = 2.5 \times 10^5\ \text{m}^{-1}$. It is noted that the absorption coefficient of the solid SiC increases by elevating the temperature from room temperature to melting temperature and that the estimated value of the absorption coefficient should fall in a value within this temperature range.

3. Free carrier absorption

In this section, the mechanism and characteristics of the absorption coefficient of solid SiC will be discussed. As bandgap of SiC is 3 times higher than photon energy of the fundamental wavelength, the intrinsic absorption of the radiation cannot be expected. In this case, the principal mechanism for radiation absorption in SiC is absorption by free charge carriers [18]. The coefficient of radiation absorption by free carriers is of the form [18]:

$$\alpha(T, N_D) = \frac{\rho e^3 \lambda^2}{4\pi^2 (m^*)^2 \varepsilon_0 n \mu} \tag{8}$$

Here ρ is the free charge carrier concentration; N_D is the impurity concentration; m^* and μ are the charge carrier effective mass and mobility, respectively; n is the refractive index; ε_0 is the permittivity; e is the electron charge; c is the speed of light. It is worth to note that both of free charge carrier concentration and mobility depend strongly on impurity concentration and temperature. To calculate the carriers concentration a two-level N donor ionization structure [19] with equal concentrations of hexagonal 0.050 eV and cubic 0.080 eV sites is used. In this work, we used an exact numerical method for calculating carrier concentration in semiconductor proposed by Abe [20], which is including the effect of Fermi–Dirac statistic for degenerate doping, temperature dependences of bandgap and band-edge tail due to random impurity potentials.

To calculate charge carrier mobility as a function of temperature and the impurity concentration, a model developed by Roschke et al. [21] is used.

$$\mu = \mu_{\min} + \frac{\mu_{\max} - \mu_{\min}}{1 + (N_D/N_{ref})^{\gamma}} \tag{9}$$

Fig. 3 illustrates the free charge carrier concentration as a function of temperature at the different level of doping concentration. Free charge carrier concentration increases with the increasing of doping level. At low doping levels ($N_D = 10^{18}$–$10^{19}\ \text{cm}^{-3}$) and low temperature field (~2000 K) free charge carriers concentration is governed by the ionization of impurity nitrogen. It increases sharply until the donor level carriers are completely excited (around temperature of 600–700 K) with the increase of temperature. Beyond this temperature range, free charge carrier concentration is saturated. At high temperature field (>2000 K), free charge carriers concentration is governed by the thermal ionization of electron in valance band. It increases again with increasing of temperature. At high doping levels ($N_D = 10^{20}$–$10^{21}\ \text{cm}^{-3}$), free charge carriers concentration is governed by the ionization of doped nitrogen over the temperature range from 300–3100 K.

Fig. 4 illustrates the free charge carrier absorption coefficient of solid SiC at fundamental wavelength (1064 nm) as a function of temperature at different levels of doping concentration. The behavior of absorption coefficient curve is almost dominated by the behavior of free carrier concentration. At low doping levels, absorption coefficient increases 3 orders due to the laser heating and the resulting temperature rise. On the other hand, absorption coefficient only increases about 2 orders at high doping level.

In this work, the ablation threshold of SiC depends strongly on the doping concentration on the wafer surface. Fig. 5 shows the absorption coefficient on the surface of SiC as a function of

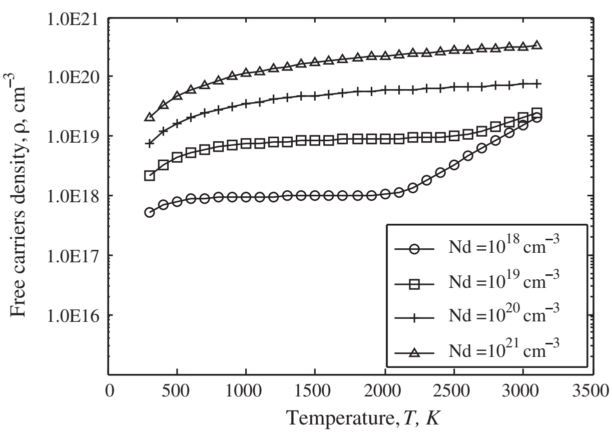

Fig. 3. Plot of free charge carrier concentration as a function of temperature at different level of doping concentration.

Author's personal copy

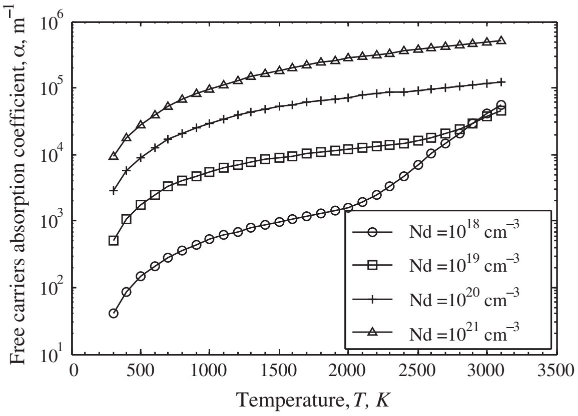

Fig. 4. Plot of free charge carrier absorption coefficient as a function of temperature at different level of doping concentration.

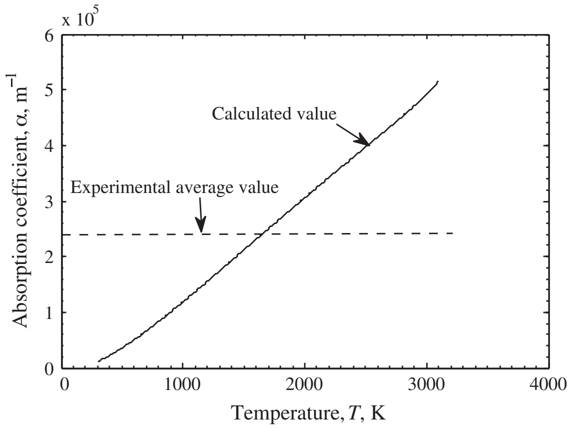

Fig. 5. Plot of absorption coefficient on the SiC surface as a function of temperature at nitrogen concentration of $1.8 \times 1020\,\text{cm}^{-3}$. Solid line represents the calculated results over the temperature range of 300–3100 K. Dashes line represents for the average value of absorption coefficient, which is predicted by experiment.

Table 1
Numerical results of average absorption coefficient over temperature range of 300–3100 K and ablation threshold of SiC at difference doping concentration level of nitrogen.

Nitrogen concentration cm^{-3}	Absorption coefficient m^{-1}	Ablation threshold J/cm^2
10^{18}	1.97×10^4	101.5
10^{19}	3.69×10^4	54.19
10^{20}	1.82×10^5	10.99
10^{21}	7.05×10^5	2.84

temperature. Dashed line shows the average value of absorption coefficient due to the laser heating of SiC wafer obtained from experiment by using following definition

$$\alpha_{\text{average}} = \frac{\int_{T_{\text{room}}}^{T_{\text{melt}}} \alpha(T)dT}{T_{\text{melt}} - T_{\text{room}}} \tag{10}$$

The calculated results show a good agreement with the experimentally obtained average value, where the average value lies within the range of the calculated value. In other words, the model of free carrier absorption coefficient can be used to estimate both average absorption coefficient and ablation threshold value. The predicted value of ablation threshold of SiC wafer for different doping level is shown in Table 1.

4. Numerical simulation of 4H–SiC ablation

In this section, a simple model is proposed that accounts for the heat conduction and the material removal due to surface evaporation to predict the cross-sectional shape of via. The energy transport for solid and liquid SiC is expressed as follows [22–23,28]:

$$\frac{\partial h}{\partial t} + v_s \frac{\partial h}{\partial z} = \frac{1}{r}\frac{\partial}{\partial r}\left(rk\frac{\partial T}{\partial r}\right) + \frac{\partial}{\partial z}\left(k\frac{\partial T}{\partial z}\right) + s \tag{11}$$

Here,

$$h = \begin{cases} \int_{T_{\text{room}}}^{T_m} C_{\text{ps}}\rho_s \mathrm{d}T & T < T_m \\ \int_{T_{\text{room}}}^{T_m} C_{\text{ps}}\rho_s \mathrm{d}T + f_l L_m & T = T_m \\ \int_{T_{\text{room}}}^{T_m} C_{\text{ps}}\rho_s \mathrm{d}T + f_l L_m + \int_{T_m}^{T} C_{\text{pl}}\rho_1 \mathrm{d}T & T > T_m \end{cases} \tag{12}$$

$$s = \alpha(T)(1-R)I_0 \exp\left(-\frac{(t-2t_0)^2}{t_0^2}\right)\exp\left(\int_0^z \alpha(T)dx\right) \tag{13}$$

Subject to the boundary conditions:

$$r = 0 : \frac{\partial T}{\partial r} = 0 \tag{14}$$

$$r \to \infty : T \to T_\infty \tag{15}$$

$$z = L : T = T_\infty \tag{16}$$

$$z = z_s : k\frac{\partial T}{\partial z} = \rho_s L_v v_s \tag{17}$$

$$t = 0 : T = T_\infty \tag{18}$$

Here, h is the enthalpy per unit volume, k the thermal conductivity, s the volumetric heat generation rate, which generated by absorbing laser pulse. A laser pulse is assumed to have Gaussian distribution in both spatial and temporal space. I_0 is the peak power of laser pulse, t_0 the pulse width, r_0 the beam waist radius, α the absorption coefficient, R the reflectivity, L the thickness of SiC wafer, z_s the surface position, L_v the latent heat of vaporization, and v_s the surface recession velocity. The surface vaporization is governed by Clausius–Clapeyron equation:

$$v_s = 0.82\frac{P_a \exp\left(\frac{L_m}{R_v}\left(\frac{1}{T_m} - \frac{1}{T_s}\right)\right)}{\rho_l\sqrt{2\pi k_B T_s/m}} \tag{18}$$

Here, P_a is the ambient pressure, L_m the latent heat of melting, R_v the universal gas constant, T_m the melting temperature, T_s the surface temperature, ρ_l the density of liquid SiC, and k_B the Boltzmann constant. Thermal properties of SiC and Si can be found in Ref. [22–24,28]

A change of optical parameter of SiC at melting temperature is taken into account. Under the melting temperature, the average absorption coefficient obtained from experiment is used. Above the melting temperature, SiC becomes a solution of carbon in liquid silicon, and the optical and thermal parameters of liquid SiC is represented by those of liquid silicon [22,24]. A change in the optical properties of the liquid silicon can occur again when the sample is heated near the critical state. When the temperature reaches $0.9T_c$, the liquid silicon becomes transparent and the incident laser energy penetrates through this transparent layer to the underlying material [26,27]. Detail of the model for optical properties of liquid silicon can be found in Ref. [28].

Fig. 6a and b show the plots of experimental and calculated diameter and depth of ablated hole against the laser fluence. Horizontal and vertical axes show fluence and diameter (depth), respectively. A good agreement between with experimental and

Author's personal copy

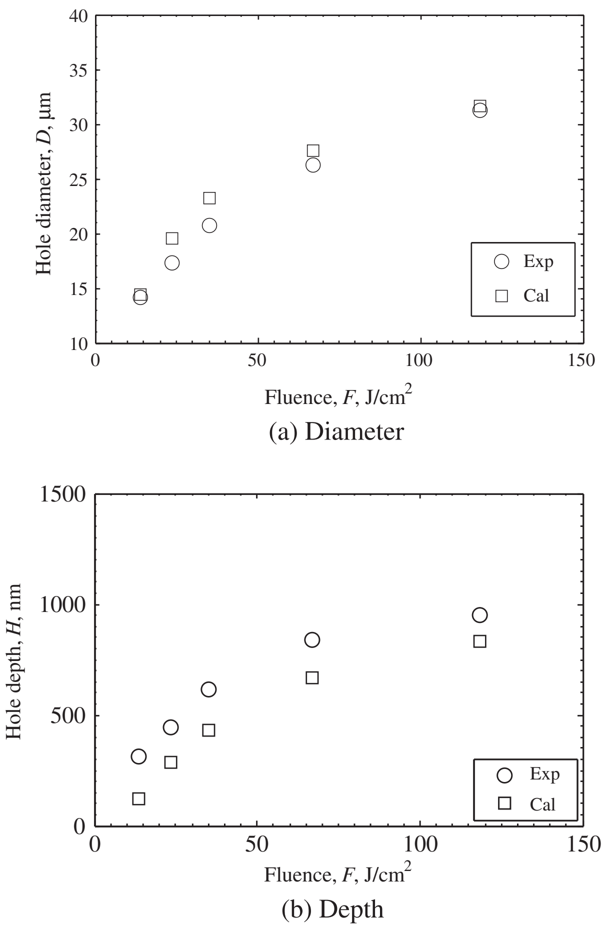

Fig. 6. Comparison of experimental and calculated diameter and depth of the ablated hole as a function of the fluence.

calculated results of diameter implies that, ablation threshold of SiC strongly depends on the nitrogen concentration of the surface and three absorption coefficient model captures very well the behavior of diameter in low fluence regime. In Fig. 6(a), calculated values are slightly larger than that of experimental results. The discrepancy can be attributed to over estimation of surface absorption coefficient of SiC.

As shown in Fig. 6(b), the experimental results of the ablation depth follow initially an exponential curve that can be explained by the variations of optical properties of SiC over the ablation process. At low fluence regime (<50 J/cm^2), the ablation process is dominated by melt ejection and surface evaporation. Major of laser pulse energy is absorbed at the liquid surface. Therefore, the fraction of pulse energy used for melt ejection and surface evaporation processes increases linearly with the increase of the laser fluence. As a consequence, ablation rate is almost constant at the low fluence regime. At the high fluence regime, however, the sample is heated near the critical state, then the liquid silicon becomes transparent and the incident laser energy penetrates through this transparent layer to the underlying material. It means that, even though the pulse energy increases, the fraction of the pulse energy used for melt ejection and surface evaporation processes does not increases significantly. Instead, more pulse energy is used to heat up the sample layer under surface and no more contributes to the ablation process. Therefore, as the intensity increases, the ablation rate decrease. In Fig. 6(b) the model underestimates the experimental data that can be due to the lack of melt ejection mode and explosion boiling mode in model.

5. Conclusion

In this work, a fundamental study about ablation threshold, absorption coefficient and absorption mechanism of silicon carbide (SiC) in the laser drilling processing is presented to figure that:According to a scale analysis, the ablation threshold value is governed by absorption coefficient of solid SiC.

The ablation threshold value and absorption coefficient of solid SiC are predicted by a single shot laser ablation experimental study: $F_{th} = 7.8\ \mathrm{J/cm^2}$, $\alpha_s = 2.5 \times 10^5\ \mathrm{m^{-1}}$. Absorption mechanism of solid SiC in infrared wavelength regime is free carriers absorption, which depend strongly on temperature.

A model, which accounts for the heat conduction, surface evaporation and the change of absorption coefficient of SiC over the temperature, captures very well the behavior of diameter and depth of ablation hole.

Acknowledgements

Part of this work has been supported by the Grant-in-Aid for JSPS Fellows from MEXT/JSPS. The authors also would like to acknowledge Tokura-Hirata laboratory for use of their AFM facility.

References

[1] P.H. Yih, A.J. Steckl, Residue-free reactive ion etching of silicon carbide in fluorinated plasmas II, J. Electrochem. Soc. 142 (2853) (1995) 312–319.
[2] J.R. Flemish, K. Xie, J.H. Zhao, Smooth etching of single crystal 6H–SiC in an electron cyclotron resonance plasma reactor, Appl. Phys. Lett. 64 (1994) 2315–2317.
[3] H. Cho, P. Leerungnawarat, D.C. Hays, S.J. Pearton, S.N.G. Chu, R.M. Strong, C.M. Zetterling, M. Òstling, F. Ren, Ultradeep, low-damage dry etching of SiC, Appl. Phys. Lett. 76 (2000) 739–741.
[4] J.J. Wang, E.S. Lambers, S.J. Pearton, M. Ostling, C.M. Zetterling, J.M. Grow, F. Ren, R.J. Shul, Inductively coupled plasma etching of bulk 6H–SiC and thin-film SiCN in NF3 chemistries, J. Vac. Sci. Technol. A 16 (1998) 2204–2209.
[5] S. Kim, B.S. Bang, F. Ren, J. D'entremond, W. Blumenfeld, T. Cordock, S.J. Pearton, SiC via holes by laser drilling, J. Electron. Mater. 33 (2004) 477–480.
[6] S. Kim, B.S. Bang, F. Ren, J. D'entremond, W. Blumenfeld, T. Cordock, S.J. Pearton, High-rate laser ablation for through-wafer via holes in SiC substrates and GaN/AlN/SiC Templates, J. Semicond. Technol. Sci. 4 (2004) 217–221.
[7] S.J. Pearton, C.R. Abernathy, B.P. Gila, F. Ren, J.M. Zavada, Y.D. Park, Enhanced functionality in GaN and SiC devices by using novel processing, Solid-State Electron. 48 (2004) 1965.
[8] Y. Dong, P. Molian, N-situ formed nanoparticles on 3C–SiC film under femtosecond pulsed laser irradiation, Phys. Status Solidi A 202 (2005) 1066–1072.
[9] Y. Dong, C.A. Zorman, P. Molian, Femtosecond pulsed micromachining of single crystalline 3C–SiC structures based on a laser-induced defect-activation process, J. Micromech. Microeng. 13 (2003) 680–685.
[10] B. Pecholt, M. Vendan, Y. Dong, P. Molian, Ultra laser micromachining of 3C–SiC thin films for MEMS device fabrication, Int. J. Adv. Manuf. Technol. 39 (2007) 239–250.
[11] S. Zoppel, M. Farsari, R. Merz, J. Zehetner, G. Stangl, G.A. Reider, C. Fotakis, Laser micro machining of 3C–SiC single crystals, Micro-Electron. Eng. 83 (2006) 1400–1402.
[12] R.F. Wood, D.H. Lowndes, Laser processing of wide bandgap semiconductors and insulators, Cryst. Lattice Defects Amorphous Mater. 12 (1985) 475–497.
[13] R. Reitano, P. Baeri, N. Marino, Excimer laser induced thermal evaporation and ablation of silicon carbide, Appl. Surf. Sci. 96–98 (1996) 302–308.
[14] Saurabh Gupta, Ben Pecholt, Pal Molian, Excimer laser ablation of single crystal 4H–SiC and 6H–SiC wafers, J. Mater. Sci. 46 (2011) 196–206.
[15] H. Howard, A.J. Conneely, G.M. O'Connor, T.J. Glynn, Investigation of a method for the determination of the focused spot size of industrial laser beams based on the drilling of holes in mylar film, in: Proceedings of Opto Ireland 2002: Optics and Photonics Technologies and Applications, vol. 4876, 2003, pp. 541–552.
[16] J. Jandeleit, A. Horn, R. Weichenhain, E.W. Kreutz, R. Poprawe, Fundamental investigations of micromachining by nano- and picosecond laser radiation, Appl. Surf. Sci. 127–129 (1998) 885–891.
[17] P. Baeri, C. Spinella, R. Reitano, Fast melting of amorphous silicon carbide induced by nanosecond laser pulse, Int. J. Thermophys. 20 (1999) 1211–1221.
[18] R.A. Smith, Semiconductors, Cambridge University Press, Cambridge, London, New York, Melbourne, 1978.
[19] C.J. Scozzie, F.B. McLean, J.M. McGarrity, Modeling the temperature response of 4H silicon carbide junction field-effect transistors, J. Appl. Phys. 81 (1997) 7687–7689.

Author's personal copy

[20] Y. Abe, An exact numerical method foe calculating Fermi energy and carrier concentration in semiconductor – an example of transcendental equation solver, Bulletin of the Faculty of Engineer Hokaido University, No. 161, 1992, Japanese.
[21] M. RoschkeLv, F. Schwierz, Electron mobility models for 4H, 6H, and 3C SiC, IEEE Trans. Electron Devices 48 (7) (2001) 1442–1447.
[22] L. Fedorenko, A. Medvid, M. Yusupov, V. Yukhimchuck, S. Krylyuk, A. Evtukh, Nanostructures on SiC surface created by laser microablation, Appl. Surf. Sci. 254 (2008) 2031–2036.
[23] Y. Gao, Y. Zhou, B. Wu, S. Tao, R.L. Jacobsen, B. Goodman, Time-resolved experimental study of silicon carbide ablation by infrared nanosecond laser pulses, J. Manuf. Sci. Eng. 133 (2011) 021006.
[24] A.N. Samant, C. Daniel, R.H. Chand, C.A. Blue, N.B. Dahotre, Computational approach to photonic drilling of silicon carbide, Int. J. Adv. Manuf. Technol. 45 (7–8) (2009) 704–713.
[25] Z. Zhang, M.F. Modest, Energy requirements for ablation or decomposition of ceramics during CO_2 and Nd:YAG laser machining, J. Laser Appl. 10 (1998) 212–218.
[26] R.O. Bell, M. Toulemonde, P. Siffert, Calculated temperature distribution during laser annealing in silicon and cadmium telluride, Appl. Phys. 19 (1979) 313.
[27] I. Lukes, R. Sasik, R. Cerny, Study of excimer laser induced melting and solidification of Si by time-resolved reflectivity measurements, Appl. Phys. A: Solids Surf. 54 (1992) 327.
[28] J.H. Yoo, S.H. Jeong, R. Greif, R.E. Russo, Explosive change in crater properties during high power nanosecond laser ablation of silicon, J. Appl. Phys. 88 (2000) 1638.